EFDA–JET–CP(09)05/09

M.-L. Mayoral, J. Ongena, A. Argouarch, Yu. Baranov, T. Blackman, V. Bobkov, R. Budny, L. Colas, A. Czarnecka, L. Delpech, F. Durodié, A. Ekedahl, M.Gauthier, M.Goniche, R. Goulding, M. Graham, J. Hillairet, S. Huygen, Ph. Jacquet, T. Johnson, V. Kiptily, K. Kirov, M. Laxåback, E. Lerche, J. Mailloux, I. Monakhov, M.F.F Nave, M. Nightingale, V. Plyusnin, V. Petrzilka, F. Rimini, D. Van Eester, A.Whitehurst, E. Wooldridge, M.Vrancken, JET-EFDA Task Force H
and JET EFDA contributors

Overview of Recent Results on Heating and Current Drive in the JET Tokamak

Overview of Recent Results on Heating and Current Drive in the JET Tokamak

M.-L. Mayoral[1], J. Ongena[2], A. Argouarch[3], Yu. Baranov[1], T. Blackman[1], V. Bobkov[4], R. Budny[5], L. Colas[3], A. Czarnecka[6], L. Delpech[3], F. Durodié[3], A. Ekedahl[3], M.Gauthier[9], M.Goniche[3], R. Goulding[7], M. Graham[1], J. Hillairet[3], S. Huygen[2], Ph. Jacquet[1], T. Johnson[8], V. Kiptily[1], K. Kirov[1], M. Laxåback[8,9], E. Lerche[2], J. Mailloux[1], I. Monakhov[1], M.F.F Nave[10], M. Nightingale[1], V. Plyusnin[10], V. Petrzilka[11], F. Rimini[9], D. Van Eester[2], A.Whitehurst[1], E. Wooldridge[1], M.Vrancken[2], JET-EFDA Task Force H and JET EFDA contributors*

JET-EFDA, Culham Science Centre, OX14 3DB, Abingdon, UK

[1]EURATOM-UKAEA Fusion Association, Culham Science Centre, OX14 3DB, Abingdon, OXON, UK
[2]Association "EURATOM - Belgian State" Laboratory for Plasma Physics Koninklijke Militaire School - Ecole Royale Militaire B-1000 Brussels Belgium, TEC Partner
[3]Association EURATOM-CEA, CEA/DSM/IRFM, Cadarache, Saint Paul Lez Durance, France
[4]Max-Planck-Institut für Plasmaphysik, EURATOM-Assoziation, D-85748 Garching, Germany
[5]Princeton Plasma Physics Laboratory, James Forrestal Campus, New Jersey, USA
[6]Association Euratom-IPPLM, Hery 23, 01-497 Warsaw, Poland
[7]Oak Ridge National Laboratory, Oak Ridge, TN 37831-6169, Tennessee, USA
[h]Association EURATOM-VR, Fusion Plasma Physics, EES, KTH, SE-10044 Stockholm, Sweden
[9]EFDA Close Support Unit, Culham Science Centre, Culham, OX14 3DB, UK
[10]Associação EURATOM/IST, Instituto de Plasmas e Fusão Nuclear, Lisbon, Portugal
[11]Association EURATOM-IPP.CR, Institute of Plasma Physics, Praha, Czech Republic
** See annex of F. Romanelli et al, "Overview of JET Results", (Proc. 22 [nd] IAEA Fusion Energy Conference, Geneva, Switzerland (2008)).*

Preprint of Paper to be submitted for publication in Proceedings of the
18th Topical Conference on Radio Frequency Power in Plasmas, Gent, Belgium.
(22nd June 2009 - 24th June 2009)

ABSTRACT.
In this paper, significant results in the heating and current drive domains obtained at JET in the past few years following systems upgrade and dedicated experimental time, will be reviewed. Firstly, an overview of the new Ion Cyclotron Resonance Frequency (ICRF) heating capabilities will be presented i.e. results from the ITER-Like ICRF antenna (ILA), the use of External Conjugate-T and 3dB hybrid couplers to increase the ICRF power during ELMy H-mode. Furthermore, experiments to study the influence of the phasing of the ICRF antenna on power absorption and coupling will be described. Looking at Low Hybrid (LH) issues for ITER, the effect of the location of gas injection on the LH coupling improvement at large launcher-separatrix distances will be discussed as the possibility to operate at ITER-relevant power densities. Experiments to characterise the LH power losses in the Scrape-Off-Layer (SOL) and to determine the LH wave absorption and current drive using power modulation will be shown. Finally, plasma rotation studies in the presence of ICRF heating with standard and enhanced JET toroidal field ripple will be presented.

1. ICRF HEATING STUDIES

1.1 THE JET ITER-LIKE ICRF ANTENNA (ILA)

The ILA was installed on JET in 2007 (see Fig.1) after commissioning on the JET test bed [1]. The ILA consists in a compact array of 8 straps combined in 4 Resonant Double Loops (RDLs) (see Fig. 1). The ILA was operated in dipole phasing (maximum parallel wave number $k_{||} \sim 8\ m^{-1}$) and at 33 and 42 MHz (the frequency range available is 30 to 49MHz) with power densities up to 6.2 MW/m^2 [2]. The ILA heating efficiency (0.8-0.9) was found to be similar to that of the A2s antennas when operated with a similar spectrum [3][4]. No deleterious effect on impurities production was observed. Figure 2 shows an example with 4.3MW of ICRF power coupled from the ILA in L-mode using H minority heating in D plasma. Note in particular the sawtooth behavior in the electron temperature, which is characteristic of a central fast ion population. The maximum power coupled achieved was 4.8MW in L-mode. Higher power was not reached due to limitation in the available generated power. Another ILA feature is its capability to couple power during the strong loading variations associated with ELMs, by controlling the impedance at the 4 T-junction points (by changing the in-vacuum capacitor values) and the 2nd stage matching settings (see Fig.1 and [5][6]). Figure 3 shows an example of an ELMy discharge with 1.8MW provided by the ILA upper half. Finally, arc detection systems relying on scattering matrix consistency check (SMAD) and sub harmonic measurements (SHAD) were developed [7] [8] in order to safely operate the ILA and avoid in particular undetected arc at the T-junctions. Aspects relevant for the design of the ICRF antennas on ITER (including coupling characterisation) and addressed by the ILA are described in [9].

1.2. ELM TOLERANCE USING A2 ANTENNAS

Following a successful proof-of-principle test [10], an External Conjugate-T (ECT) layout was installed in 2008 between the A2 antennas C and D (see Fig.1). For the ECT, phase shifters are used

in order to control the T-junction impedance. The commissioning that started beginning of 2009 was found remarkably straightforward and reliable performances were obtained with up to 4 MW of ICRF into ELMy H-mode plasmas[11]. For the ECT, arc protection was efficiently insured by the newly implemented Advanced Wave Amplitude Comparison system (AWACs) [10]. Moreover, the ELM tolerance provided by the 3dB hybrid couplers installed between the A2 antennas A and B in 2005 and commissioned in 2006 [12], was further improved by new modifications in the arc detection system (based of voltage standing wave ratio measurements). In this way, the coupled power was safely increased up to 3MW. As a result, the four A2 antennas together (conditioned up to 30kV) can now couple up to 7 MW in a wide range of H-mode plasmas, including Type I ELMs.

1.3. HEATING EFFICIENCY AND EDGE INTERACTION FOR DIFFERENT PHASINGS OF THE ICRF A2 ANTENNA STRAPS

A dedicated study was carried out to assess the influence of the relative phasing of the A2 antenna straps on coupling of ICRF power to the plasma and hot-spot formation on first wall components. Although this topic is not new [13], it was only partly studied in the past. Moreover, the presence of new diagnostics recently installed at JET rendered it worthwhile to readdress this problem and allowed to obtain a much better documentation of the wall interaction than was previously possible. Optimizing ICRF power absorption consists in maximizing conditions with inverse dependence on $k_{||}$ i.e. (i) the propagation through the evanescence layer $\propto \exp(-\alpha k_{||} x)$, with x the width of the evanescent zone and α the tunnelling coefficient, (ii) the cut-off density value $n_{e,cut\text{-}off}\ \alpha k^2_{||}$ and (iii) the ICRF wave absorption in the plasma. While conditions (i) and (ii) both favour small k// values, condition (iii) favours large $k_{||}$ values. The present experiments were performed in L-mode plasmas with magnetic field of B_t = 3.0T and plasma current I_p = 2.0MA, heated with ~4MW of ICRF power at 42MHz (H minority heating, H concentration ~ 7%) delivered by the 4 straps A2 antennas A, B and C [3]. The distance between the separatrix and the antenna straps was the same for all discharges and fixed at 11.0±0.5cm. The phase of the straps was varied between (0ππ0), (00ππ) and (0π0π) giving respectively dominant $k_{||}$ values of ~2.5m^{-1}, 4m^{-1} and 6.5m^{-1}. Fig. 4 summarizes the main results. Although the best coupling (see Fig.4e) was obtained for the super dipole (00ππ) case, this phasing led to much larger interaction with the first wall. Indeed, bright hot spots were observed both with the visible and the infra-red camera with temperatures at the septum of antenna A (Fig.4d) appreciably higher. Modelling by the 1D wave code TOMCAT [14], shown that the estimated double pass absorption with the super-dipole phasing], larger enhanced radiated power due to higher impurity content in the plasma [] and enhanced excitation of coaxial modes []. was about 44% compared to 89% and 75% for the (0π0π) and (0ππ0) phasings, in line with the heating efficiencies deduced from break-in slope analysis of the diamagnetic plasma energy. The loss mechanisms for the (00ππ) phasing can be related to enhanced RF sheath rectification [15], larger enhanced radiated power due to higher impurity content in the plasma [4] and enhanced excitation of coaxial mode [16].

2. LH HEATING AND CURENT DRIVE STUDIES

2.2 INFLUENCE OF GAS INJECTION LOCATION ON LH WAVE COUPLING

Good coupling of the LH wave in H-mode plasmas in JET, at large distance between the separatrix and the launcher, can be obtained using the dedicated gas injection system located near the launcher (named GIM6) [17, 18, 19]. In view of the use of LHCD in ITER, an experiment was carried out to assess the possibility of using the gas injection locations as those foreseen for fuelling in ITER, i.e. from the top ports. The LH reflection coefficients were compared in otherwise identical discharges, in which only the gas injection location was varied. The plasma scenario was a Type I ELMy H-mode plasma with H98(y,2) ~ 1.0. The distance between the separatrix and the launcher was varied between 8 and 10cm. To obtain identical initial conditions for the LH coupling in all discharges, the near gas injection valve (GIM6) was used during the initial LH power application. The gas injection location was then switched 0.5 s after the start of the LH power. As can be seen in Fig.5, the LH power reflection coefficient, averaged over the whole launcher, increased from 3% to > 10%, as soon as GIM6 was stopped and a top gas injection valve was used. In the configuration chosen, GIM7 (225^{o} toroidally from the LH launcher) was magnetically connected to the whole launcher, while GIM8 (135° toroidally from the launcher) was only connected to the upper part of the launcher. Even though from GIM6, and even though the top gas injection valves were magnetically connected to the launcher, GIM6 was still clearly more efficient than the gas inlets located at the top. Essentially, the result obtained with a non-connected top gas injection valve was the same as the result with the connected one. At the present state, the conclusion would be that the LH system in ITER would need a dedicated gas injection system, located at the outer mid plane close to the LH launcher and that it would not be sufficient to rely on the main gas injection from the top ports. Nevertheless, further experiments using different plasma equilibria and magnetic connections between gas injection points and the launcher should be preformed to substantiate these results.

2.3. TOWARDS ITER-LIKE LH POWER DENSITIES

A dedicated effort has been undertaken in the 2008 JET experimental work plan to increase the launched LH power density towards the ITER value (24MW/m^2 for 3.7GHz), and investigate any limitations. The LH launcher waveguides were conditioned by applying short bursts of power on vacuum, followed by series of shots on plasma with good coupling conditions and with the launched power and the duration of the LH phase gradually increased to allow for out-gassing of the waveguides. ITER power densities have been reached in this way, with no other limitation than that of conditioning (this is made worse by the fact that the waveguides are not actively cooled hence their temperature increases shot by shot, and leads to enhanced out-gassing). An example is shown in Fig.6 demonstrating that stationary conditions were reached for up to 6s at these high power densities without detrimental effects on the launcher, as evidenced by the stationary radiated power. These results were obtained for distances between the launcher grill mouth and the plasma separatrix of up to 10cm and local gas puff from GIM6 to obtain good coupling conditions, as described

above. Finally, note that this dedicated conditioning time led to 5.7MW of LH coupled in L-mode, a record value in the last 10 years.

2.4 CHARACTERISATION OF LH POWER LOSSES IN FRONT OF THE LAUNCHER

Under the conditions mentioned in the previous paragraph, LH power absorption in the SOL was studied in JET using Infrared thermography [20]. Hot spots due to the generation of fast electrons by the LH wave in the SOL [21] were observed on poloidal limiters or dump plates located at the top of the plasma chamber. The power density flowing along the field lines generating the hot spots was estimated to be about 10MW/m^2 in these conditions. By varying the launcher position, (retracting it away from a starting position close to the plasma, (see Fig.6e)), such that the radial distance between the field lines (generating the hot spots on the dump plates) and the launcher was increased from 0 to 3.5cm, it was possible to diagnose the radial width of the absorption layer in front of the launcher. By analysing the temperature evolution of hot spots on the dump plates (see Fig.6e)), the LH power dissipation layer in front of the grill was inferred to be at least 3.5cm. This is in agreement with recent observations on Tore Supra [22], but not with the standard modelling of the linear damping of LH waves in the SOL that predicts a dissipation layer of a few mm. These Tore Supra and JET results have triggered new modelling efforts to better describe the absorption of LH waves with the SOL [23][24].

2.5. LH WAVE ABSORPTION & CURRENT DRIVE STUDIES USING POWER MODULATION

LH wave absorption and current drive studies were performed using LH power modulated at a frequency ω_0 and Fast Fourier Transform analysis of the response in the electron temperature [25], measured from ECE emissions. Note that the optical thickness of the plasma in most of the experiments was sufficiently large in the region of interest [26]. Up to 4MW of square modulated (70-90%, 42Hz) LH power was used. Scan in plasma density (from 1.5 10^{19} m^{-3} to 5 10^{19} m^{-3}) and magnetic field (2.2, 2.7 and 3.4T) were performed. The relation between the modulated power and the T_e response is not trivial as heat transport between the LH fast electrons and the bulk plasma ones, has to be taken into account. Modelling using the TRANSP and JETTO transport codes has shown that *max($\delta\phi$)*, the maximum in the phase difference between the first harmonic of the modulated LH power $P_{LH}(\omega_0)$ and the measured electron temperature $T_e(\omega_0)$ could be used to assess the current drive efficiency and LH power deposition [27), that is closely related to the peak in the LH deposition profiles, was found to move toward the plasma periphery with increasing plasma density. This shift was very similar all the Bt values tested in the experiment. Furthermore, the behaviour of the ratio between the third and the first harmonic of the measured electron temperature $\tilde{T}_e(3\omega_0)/\tilde{T}_e(\omega_0)$, was used to assess the current drive efficiency Using a 2D relativistic Fokker-Planck code, extensive comparison between the modelled and the experimental values of $\tilde{T}_e(3\omega_0)/\tilde{T}_e(\omega_0)$, was performed. In particular, in the model, the effect of the width of the electron distribution plateau that directly related to the

current drive efficiency was scanned in order match the experimental value. For example, at high density the best agreement was found for smallest plateau width corresponding to lowest current drive efficiency [25]. Note that standard Ray-tracing / Fokker-Planck modelling performed for these experiments predicts more centrally peaked power deposition profile and higher current drive efficiencies. This discrepancy could be explained assuming that the initial LH power spectrum undergoes in the plasma a strong upshift in $N_{||}$.

7. EFFECT OF RIPPLE ON TOROIDAL ROTATION IN PLASMAS HEATED WITH ICRF

In view of its importance for ITER, the effect of toroidal field ripple amplitude δ (defined as $\delta = (B_{max} - B_{min})/(B_{max} + B_{min})$ in the equatorial plane at a major radius of 3.8m for JET) on intrinsic rotation in plasmas with no momentum input was studied. JET has 32 toroidal field coils consisting of two interleaved sets of 16 coils and the ripple amplitude δ can be varied by changing the current in the two coil sets. In the experiments described here, δ was changed from 0.08% (standard JET operation) to 1.5%. For comparison, ITER with 18 toroidal field coils will have ripple amplitude of 0.5% at the edge [28]. For δ =0.08, toroidal angular frequencies $\omega_\phi \leq$10 krad/s were found both in ohmic plasmas [29], or plasmas heated with ICRF [30,31,32] or LH [32]. At this low ripple level the edge is always co-rotating independent of the heating scenario. Rotation in the core of JET can be either in the co- or counter current direction: in ohmic plasmas the centre is counter-rotating [29][32], while with ICRF the plasma centre is either counter- or co-rotating depending on the plasma current [32] and the position of the ICRF resonance [31]. Recent results for experiment performed at plasma current of 1.5MA and magnetic field of 2.2 T for ohmic JET and ICRF heated plasmas are illustrated in Figs. 8 and 9. Hydrogen minority heating was used with the antennas in dipole phasing, and PICRF up to 4MW. Toroidal angular frequency rotation profiles were measured with Charge eXchange Recombination Spectroscopy (CXRS) of C^{+6}, with an integration time of 10ms, during short NBI pulses (blips) and rotation profiles were averaged over the first 20 ms of those blips, to minimize the influence of momentum input by NBI. In these experiments, the application of ICRF always added a counter rotation to the total rotation at all radii. Figure 8 shows that in ICRF heated plasmas with increased field ripple counter rotation increased in both plasma edge and core. This is with the ICRF resonance located off-axis (R_{res} = 2.71m) to the high field side. However, for a fixed ripple value of 1.5%, larger values for edge and core counter rotation were observed when the ICRF resonance position was moved further to the low-field side (R_{res} = 2.38m, 2.71m and 3.13m), as illustrated in Fig.9 .These new results not fully understood are currently modelled using the SELFO code.

CONCLUSIONS

The upgrade of the JET ICRF system has confirmed that coupling ICRF power during ẼLMs is now a problem solved. Two main EL̃M tolerant systems were tested: 3dB hybrid couplers (confirmation of ASDEX results [33]), and conjugate-T layout with internal (in-vacuum capacitor for the ILA) or external (phase shifters), matching elements. The availability of this increased

amounts of ICRF power in H-mode, was heavily used in the last JET experimental campaign. For examples, up to 7.5MW were coupled to reach a total additional power above 26MW in high performance plasmas (β_N up to 3.1) and H98(y,2) (up to 1.37) [34] and up to 8.5MW were coupled in experiments aiming at comparing NBI/ICRF H-modes. The effect of different antenna phasing, similar to the ones foreseen in ITER, shown that (00ππ) phasing leads to reduced power coupling to the plasma and increased edge interaction to the plasma compared to (0π0π) and (0ππ0) phasings. The coupled LH power was maximised by thoroughly conditioning the launcher leading to ITER like power densities (24MW/m^2). Gas puffing studies indicated that fuelling from a distant gas inlet was not very efficient to improve the LH coupling even if magnetically connected to the launcher, and that a dedicated gas pipe is likely to be a necessity for the LH system on ITER. New experimental techniques based on thermography analysis and LH power modulation, were developed to further investigate LH wave absorption mechanism. Finally, rotation in ICRF heated plasmas was found to be not only affected by ripple but also on the position of the ICRF resonance in the plasma.

ACKNOWLEDGMENTS

This work was partly funded by the United Kingdom Engineering and Physical Sciences Research Council and by the European Communities under the contract of Association between EURATOM and UKAEA and was carried out within the framework of the European Fusion Development Agreement. The views and opinions expressed herein do not necessarily reflect those of the European Commission.

REFERENCES

[1]. F. Durodié et al., Fusion Engineering Design **84**, 279-283 (2009)
[2]. F. Durodié et al., contribution A21, this conference
[3]. A. Kaye et al., Fusion Eng. and Design, **74**, 1-21 (1994).
[4]. E. Lerche et al., contribution B30, this conference
[5]. M. Vrancken et al. , contribution B43, this conference
[6]. D. Van Eester et al., contribution B41, this conference
[7]. M. Vrancken et al., contribution A45, this conference
[8]. P. Jacquet et al.,, contribution B26, this conference
[9]. M. Nightingale et al., invited talk I30, this conference
[10]. I. Monakhov et al., in Radio Frequency Power in Plasmas, edited by P. M. Ryan and D. A. Rasmussen, AIP Conference Proceedings 933, Melville, New York, 2007, pp.147-150.
[11]. I. Monakhov et al., contribution A33, this conference
[12], M.-L. Mayoral et al., in Radio Frequency Power in Plasmas, edited by P.M. Ryan and D.A. Rasmussen, AIP Conference Proceedings 933, Melville, New York, 2007, pp.143-146.
[13]. A. Kaye et al., Fusion Engineering 1995 SOFE, 16th IEEE/NPSS Symposium **V1**, 736-741 (1995)
[14]. D. Van Eester and R. Koch, Plasma Phys. Contr. Fusion, **40,** 432 (2006)
[15]. V. Bobkov et al.,, invited talk I3, this conference

[16]. R. Weynants et al., Review Talk R1, this conference.
[17]. A. Ekedahl et al., Nuclear Fusion **45,** 351 (2005)
[18]. A. Ekedahl et al., Plasma Phys. Control. Fusion **51**, 044001 (2009)
[19]. M. Goniche et al., Plasma Phys. Control. Fusion **51**, 044002 (2009)
[20]. P. Jacquet et al., this conference.
[21]. V. Fuchs et al., Phys. Plasmas 3, 4023 (1996).
[22]. J. Gunn et al., J. Nucl. Mat. **390-391**, 904 (2009).
[23]. V. Fuchs V. et al., contribution A52, this conference.
[24]. V. Petrzilka et al., EPS Conference proceedings, Sofia (2009)
[25]. Y. Baranov et al, contribution A48, this conference.
[26]. C. Sozzi et al., this conference
[27]. K. Kirov, EPS proceedings, Bulgaria, Sofia (2009)
[28]. A. Fasoli et al, Nucl. Fusion **47**, S264 (2007)
[29]. M.F.F. Nave et al, 34th EPS Conf., Warsaw, Poland (2007), contribution P-4.158
[30]. L.-G. Eriksson, E. Righi and K-D Zastrow, Plasma Phys. Contr. Fusion **39**, 27 (1997)
[31]. L.-G. Eriksson et al., Plasma Phys. Control. Fusion **51,** 044008 (2009)
[32]. J.-M. Noterdaeme et al. Nucl. Fusion **43**, 274 (2003)
[33]. J.M Noterdaeme et al., Fusion Eng. Design, **74,** 191-198 (2005)
[34]. J. Mailloux, EPS, Sofia, Bulgaria, (2009)

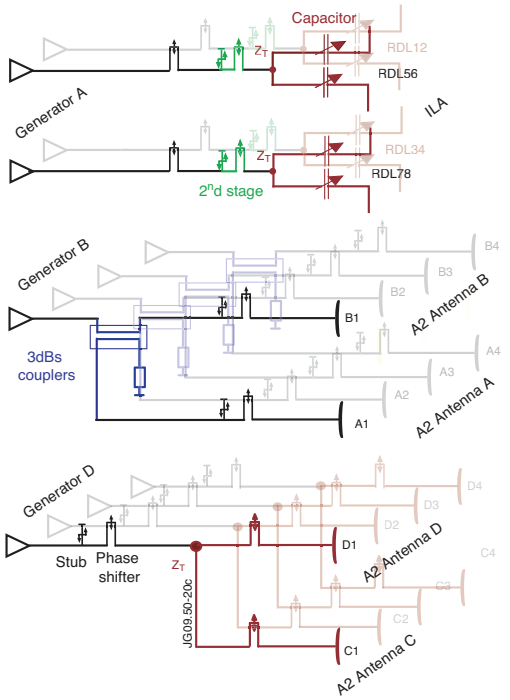

Figure 1: Schematic overview of the present ICRF system on JET in its ELM-tolerant mode.

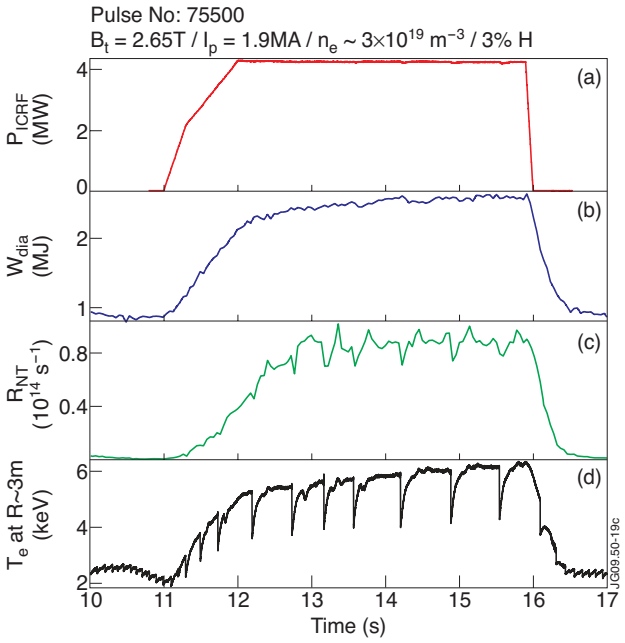

Figure 2: Time evolution of (a) ILA ICRF power, (b) diamagnetic energy, (c) neutron rate and (d) central electron temperature (from top to bottom). The ICRF heating scheme used was H minority in D.

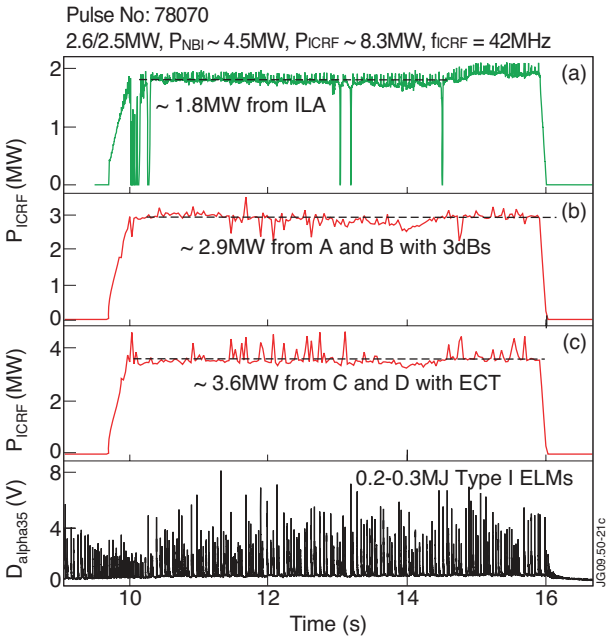

Figure 3: Example of ELMy H-mode with high level, 8.3MW, of ICRF power coupled. The time evolution of the power coupled from (a) the 2 upper RDLs of the ILA (equipped with in vacuum conjugate-T, (b), antennas A and B (equipped with 3dB couplers), (c) antennas C and D (equipped with external conjugate T) is represented.

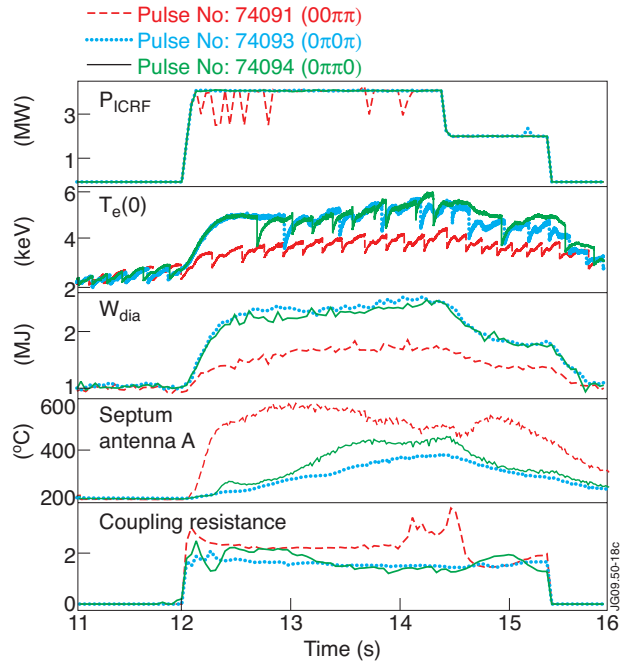

Figure 4: Time evolution of (a) the ICRF power, (b) the central electron temperature, (c) the diamagnetic energy, (d) the maximum temperature of antenna A septum and (f) the antenna B strap averaged coupling resistance for different A2 antennas phasings: 00ππ (Pulse No: 74091), 0π0π (Pulse No: 74093) and 0ππ0 (Pulse No: 74094)

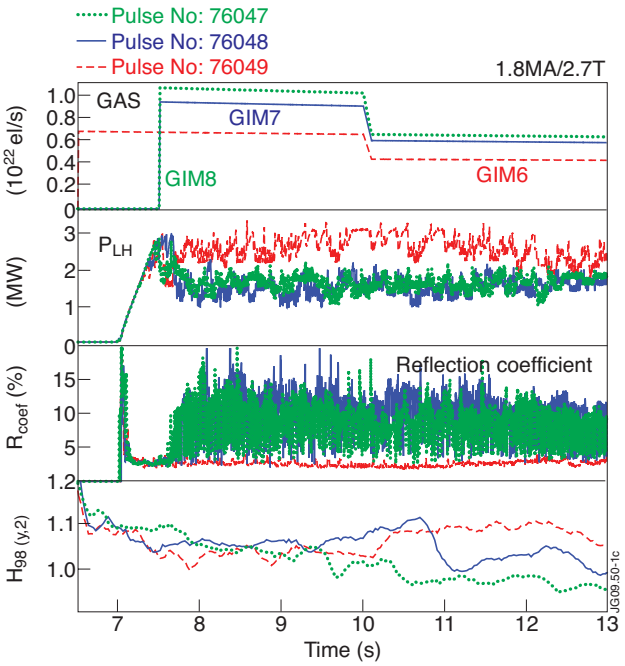

Figure 5: Time evolution of (a) the gas injection rate, (b) the LH power, (c) the reflection coefficient and (d) the confinement factor H98(y,2) for three pulses each with gas injection from different location: GIM6 (midplane near the launcher) for Pulse No: 76047, GIM7 (top of chamber and magnetically connected to launcher) for Pulse No: 76048, GIM8 (top of chamber but marginally connected to the launcher) for Pulse No: 76050.

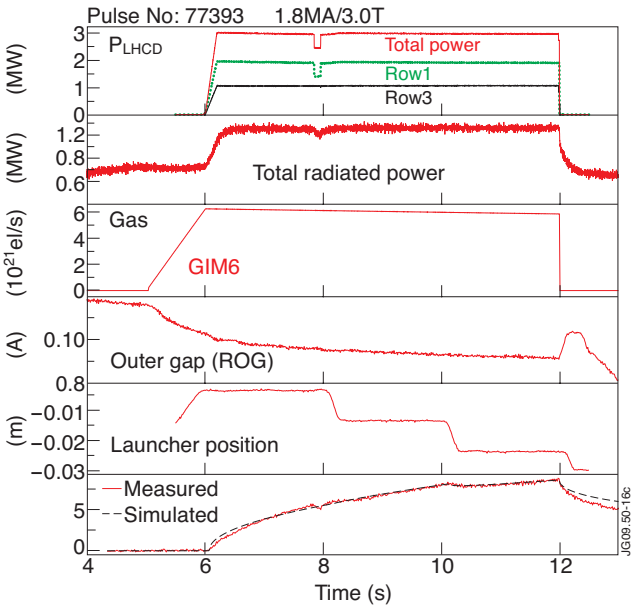

Figure 6: Time evolution of the LH power (top row 1 plus bottom row 3), total radiated power, gas injection rate from GIM6, separatrix - poloidal limiters distance, launcher front – poloidal limiter distance, temperature evolution of LH hot spot measured on dump plates. In this pulse, an ITER-like power density of ~ 24MW/m^2 were reached on both rows.

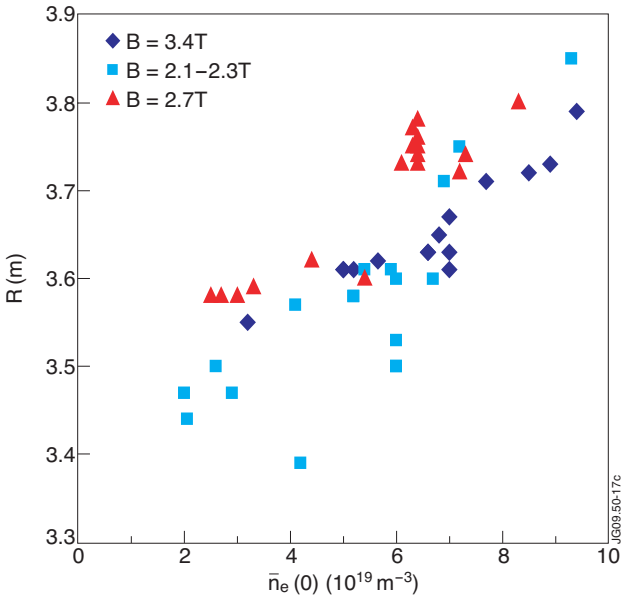

Figure 7: Position of the maximum phase difference $\delta\Phi$ versus line averaged density, for different values of B_t : squares B_t=2.1-2.3T, triangles B_t = 2.7T, diamonds B_t =3.4T.

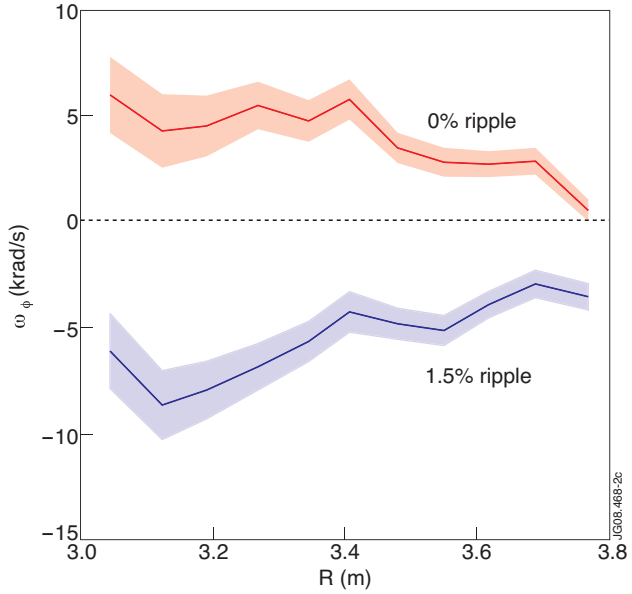

Figure 8: Toroidal rotation profiles for ICRF heated plasmas at 2.2T/1.5MA and two ripple levels. Top: Pulse No: 74688 with ~ 0% ripple (0.08) and P_{ICRF} = 3.1MW; bottom: Pulse No: 74686 with 1.5% ripple and P_{ICRF} = 2.9MW. The plasma centre is at 3.02m, the ICRF resonance is located at 2.71m.

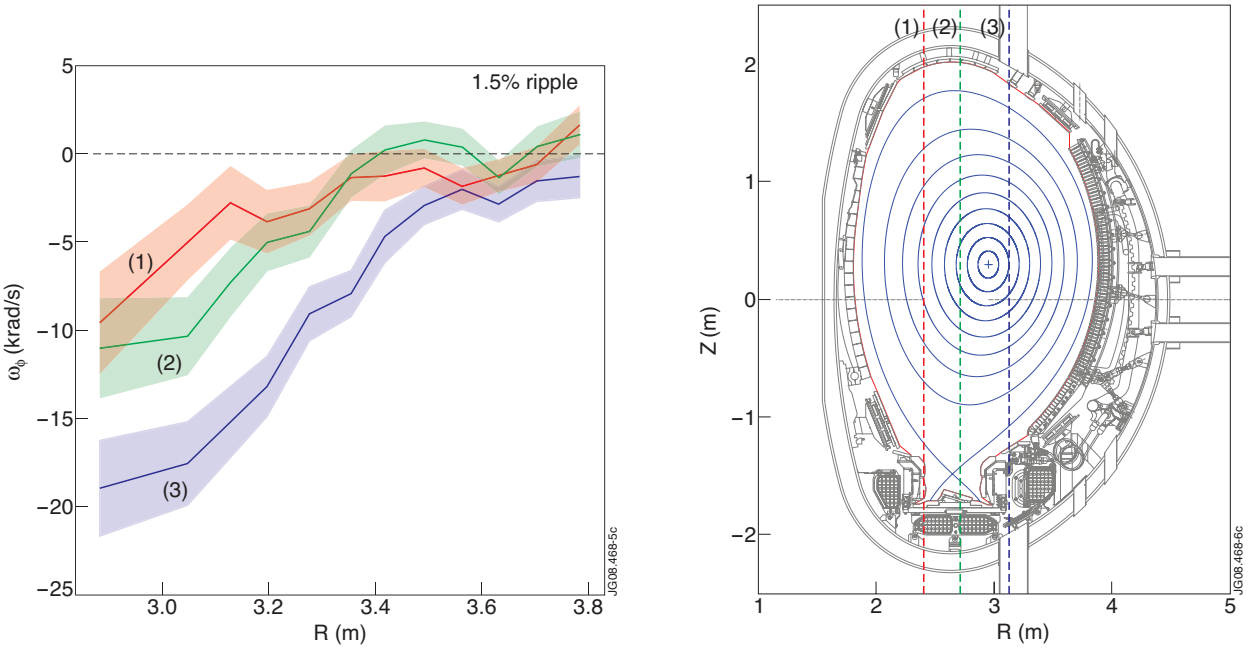

Figure 9: Toroidal rotation profiles for pulses at 2.2T/1.5MA with 1.5% ripple and P_{ICRF}~2MW, for three different resonance positions: (1) Pulse No: 77010 with R_{res}=2.38 m, (2) Pulse No: 77014 with R_{res}=2.71m, (3) Pulse No: 77009 with R_{res}=3.13m. The resonance positions are shown in the insert.